A study of cosmic ray muons above 10^{13} eV by observation of horizontal air showers

1973 J. Phys. A: Math. Nucl. Gen. 6 1262

(http://iopscience.iop.org/0301-0015/6/8/019)

J. Phys. A: Math., Nucl. Gen., Vol. 6, August 1973. Printed in Great Britain.

A study on cosmic ray muons above 10^{13} eV by observation of horizontal air showers

E Böhm and M Nagano†

Institut für Reine und Angewandte Kernphysik der Universität Kiel, Kiel, West Germany

Received 16 February 1973

Abstract. The study of horizontal air showers (HAS) has been continued at Kiel with improved resolution in zenith angle determination. The zenith angle distribution of HAS is consistent with the $\sec\theta$ distribution of muons in the size region between $2{\cdot}5\times10^3$ and $3{\cdot}1\times10^4$. The integral size spectrum is $I(\geqslant N, \geqslant 70°) = (1{\cdot}3\pm0{\cdot}4)\times10^{-13}(N/10^4)^{-2{\cdot}4\pm0{\cdot}2}$ $\mathrm{cm}^{-2}\,\mathrm{s}^{-1}\,\mathrm{sr}^{-1}$ and is in agreement with the spectrum produced by muon bremsstrahlung as calculated by Király *et al* up to the shower size of 5×10^4 within the experimental uncertainties. These results can be explained with the conventional model of muon production through pion decay (and to some extent through kaon decay) up to a muon energy of about 5×10^{13} eV. The number of muons observed in HAS is one order of magnitude larger than would be expected from the above bremsstrahlung hypothesis. The possibility of these muons being produced in HAS is discussed and methods of discrimination of remnant muons produced in EAS are presented. The upper limit of the flux of an isotropic component of muons or of heavy mass particles is discussed.

1. Introduction

Usually extensive air showers observed at sea level with zenith angles larger than about 70° are called horizontal air showers (HAS) and they are distinguished from 'ordinary' extensive air showers (EAS). Because of the large atmospheric depth in the horizontal direction, the electromagnetic and hadronic component in EAS is completely absorbed and hence HAS are considered to be secondary showers produced by the penetrating component. The main questions on HAS are: (i) the kind of parent particle; (ii) the production process of the parent particle; and (iii) the production process of the HAS. The conventional answer to these questions is that HAS are electromagnetic cascade showers produced by bremsstrahlung photons of muons from pion and/or kaon decay. Thus, the study of HAS is closely connected to the study of the production and interaction process of high energy cosmic ray muons above 10^{13} eV, of a hitherto inaccessible energy.

The production process of high energy cosmic ray muons has been studied by many groups, especially after the proposal of the 'X-process' by Bergeson *et al* (1967). If there is a new production process of muons, it should be possible to see it in the angular

† On leave of absence from Institute for Nuclear Study, University of Tokyo.

distribution of high energy muons. By direct measurements with magnetic spectrometers no anomalies have been observed below 1 TeV (Stefanski *et al* 1968, Asbury *et al* 1970) and above 1 TeV (Flatté *et al* 1971). In the energy region of 1–5 TeV, the zenith angle distribution has been measured by means of an emulsion chamber exposed at shallow depth (Mizutani *et al* 1971, Amineva *et al* 1971, Baradzei *et al* 1971). All these experiments are consistent with muon production from pion and kaon decay. An experiment deep underground in the Kolar gold fields (Krishnaswamy *et al* 1968) and observation of bursts produced in rock by Chin *et al* (1971) also support these results. On the contrary Bergeson *et al* (1971) need a new process in the muon energy range 1–3 TeV to explain their latest results based on measurements deep underground. Burst observations by Khristiansen *et al* (1971) at shallow depth support the existence of such a new process in the TeV energy region.

Concerning muon interactions there are no direct measurements in the energy region above a few 100 GeV due to the small flux. At higher energies muon interactions are studied in a rather indirect way by comparison of the muon energy spectrum with the depth–intensity relation of muons or burst size spectra in terms of a coefficient b in the energy loss formula for muons. b is not known very accurately: $3{\cdot}3$–$4{\cdot}1 \times 10^{-6}$ g^{-1} cm^2. The main contribution to b comes from bremsstrahlung and pair production. The contribution of the nuclear interaction is considered to be small, though some calorimeter experiments suggest an increase of the nuclear interaction cross section in the energy region above a few hundred GeV (Higashi *et al* 1961, Khristiansen *et al* 1971). But most of the experiments can be explained with a constant photonuclear cross section of 10^{-28} cm^2 up to a few TeV (Mikamo *et al* 1970).

If the conventional model for muon production and propagation in the atmosphere still holds above 10^{13} eV, we may expect, very roughly, the zenith angle distribution of HAS to be $\sec\theta$, the exponent of the size spectrum to be $\gamma - 1$ (where γ is the slope of the integral primary spectrum) and all HAS to be purely electromagnetic cascade showers. However, some doubt has arisen from various experiments in the past few years.

(i) The zenith angle distribution of HAS does not follow the $\sec\theta$ enhancement in a simple way (Hara *et al* 1970, Nagano *et al* 1971, Böhm *et al* 1970).

(ii) The shower size spectrum extends with a constant slope up to 10^5 (Hara *et al* 1970, Nagano *et al* 1971) and the flux of HAS above 10^5 is much larger than the value expected from muon bremsstrahlung (Catz *et al* 1971).

(iii) The muon content in the HAS cannot be explained by the bremsstrahlung process only (Hara *et al* 1970, Nagano *et al* 1971).

(iv) The largest HAS observed at Tokyo (INS) clearly contains a hadron and muons, suggesting the shower to be a nuclear cascade shower (Matano *et al* 1965).

In order to explain these phenomena, the proposal of the increasing muon–nucleon interaction cross section (Matano *et al* 1968, Hara *et al* 1970, Nagano *et al* 1971), and as an alternative, several proposals concerning the parent particles of HAS other than muons have been made (excited baryon, Smorodin 1966; heavy mass particle, Castagnoli *et al* 1969, Sitte 1969, Gawin *et al* 1970; heavy leptons, Pakvasa *et al* 1971; light charged particles, Dedenko and Zhelenznykh 1971).

In this paper we present further experimental results on HAS obtained at Kiel with improved resolution in zenith angle determination. The zenith angle distribution and the size spectrum of HAS will be presented and discussed. Special attention has been given to the question of the contamination of EAS to HAS observation by investigating the characteristics of inclined EAS in some detail. Methods to measure muons produced during the development of HAS are presented and the preliminary results are shown.

2. Experiment

2.1. Experimental details

The central part of the experimental array is shown in figure 1. Nine scintillation counters of 1 m^2 area are arranged in a plane tilted by 65° into a horizontal direction (horizontal array, H1–H9). Three of them (H7–H9) have been added to the previous array (Böhm

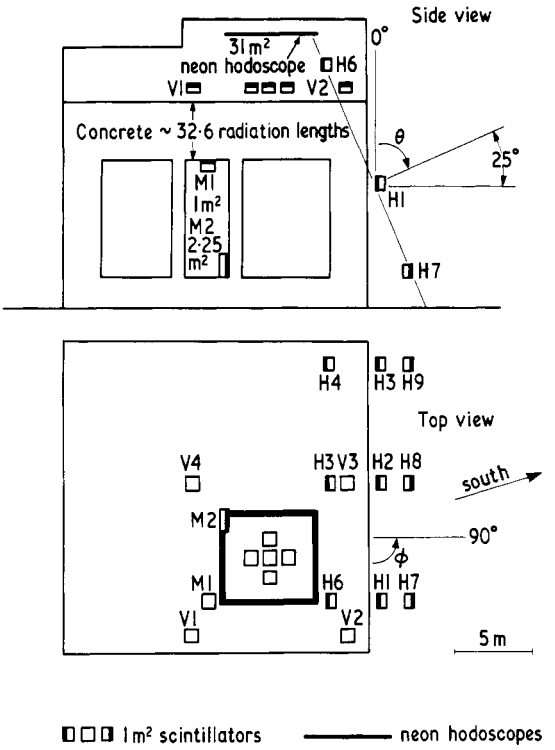

Figure 1. Arrangement of horizontal detectors and the central part of the vertical array.

et al 1971) in July 1971 in order to improve the angular resolution and the size determination. The inclination has been changed from 85° to 65° to get an angular resolution better than 5° between 40° and 90°. The scintillators are still inclined by 90° to the vertical. Both the arrival time and the density of particles are measured in each detector with photomultipliers 58AVP and 54AVP respectively. Arrival time differences are measured in the following ten combinations of detectors: H1–H2, H2–H3, H3–H4, H4–H5, H5–H6, H6–H1, H2–H5, H6–H7, H5–H8 and H4–H9. The detectors and the electronic systems are similar to those employed in the Kiel air shower array described in detail in Böhm *et al* (1966).

Additional information on the arrival time of particles and the density is provided by the vertical EAS array (vertical array, V1–V16, figure 2). There are six fast timing channels (V1–V2, V2–V3, V3–V4, V4–V1, V1–V3 and V2–V4) and sixteen density channels.

A muon detector of 1 m^2 set up under the bunker ceiling (M1) has been used to check the muon content in HAS. The arrival time difference between shower particles striking

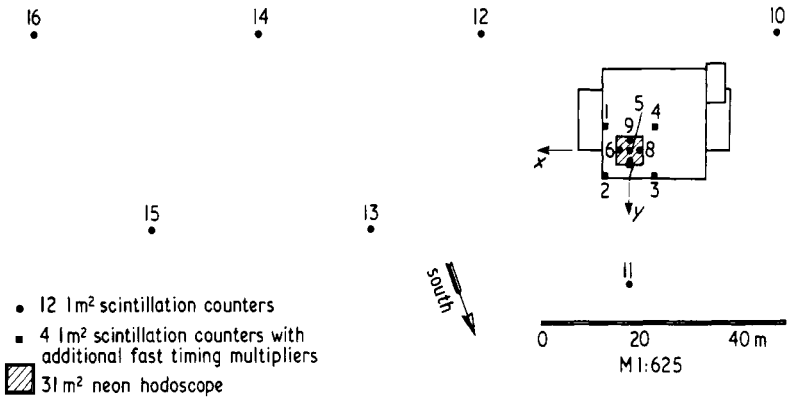

Figure 2. Arrangement of the vertical detectors.

V1 and M1 has also been recorded. The new muon detector (H2) of 2·25 m^2 has been in operation from October 1972 but has not been used for the present analysis.

The stable and reliable operation of the whole system is maintained by regular checks. The fast timing system is checked with luminescence diodes (Motorola, MV1) which are set up in all horizontal detectors (Kendziorra 1971).

A record is made whenever one of the three conditions given in table 1(*a*) is satisfied. τ_i are the delay times between particles passing the different detectors. The present analysis is based on the data from July 1971 to July 1972. The total effective running time is 6020 hours for the main run (M-run). For 450 hours τ_3, τ_4 and τ_5 in table 1(*a*) have been changed to 25 ns in table 1(*b*) in order to investigate showers of zenith angles between 35° and 65° in detail (S-run).

Table 1. Triggering conditions

(*a*) Main run (M-run): 6020 hours
Any one of the three conditions:
(i) Densities in all six detectors (H1, H2, H3, H4, H5 and H6) $\geqslant$ 1 particle
τ_1: H1–H6 $\leqslant$ 7·5 ns
τ_2: H3–H4 $\leqslant$ 7·5 ns
(ii) Densities in all six detectors (H1, H2, H5, H6, H7 and H8) $\geqslant$ 1 particle
τ_3: H7–H6 $\leqslant$ 13·5 ns
τ_4: H8–H5 $\leqslant$ 13·5 ns
(iii) Densities in all six detectors (H2, H3, H4, H5, H8 and H9) $\geqslant$ 1 particle
τ_4: H8–H5 $\leqslant$ 13·5 ns
τ_5: H9–H4 $\leqslant$ 13·5 ns
(*b*) Sub-run (S-run): 450 hours
Conditions as above except of $\tau_3, \tau_4, \tau_5 \leqslant$ 25·0 ns

2.2. *Calculation of the efficiency of shower detection*

By the present triggering requirement, the shower detection efficiency depends on both the size and the arrival direction of the shower. The calculation of such an efficiency is

divided into two parts: the calculation of the effective area A due to the particle discrimination and of the triggering probability P due to the fast timing discrimination. A depends on the shower size N, the shower age s and the arrival direction (zenith θ and azimuth ϕ). P depends in addition on the thickness of the shower disc.

The calculation of A has been made allowing for poissonian fluctuations around the average density in the effective scintillator area. The approximate expression of the Nishimura–Kamata lateral structure function given by Greisen (1956) (NKG function) has been used. Since the threshold number of particles is one in each detector, it is not necessary to consider the difference of the path lengths in the scintillator for various arrival directions.

If the uncertainty in the time measurement is expressed by the standard deviation σ of a gaussian distribution, the probability that a shower with θ and ϕ satisfies the triggering requirement is expressed by

$$P(\theta, \phi) = \frac{1}{(2\pi)^{1/2}} \int_{-\infty}^{x_0} \exp(-\tfrac{1}{2}x^2)\, dx \tag{1}$$

where

$$x = \frac{t - t_{\theta,\phi}}{\sigma} \qquad \text{and} \qquad x_0 = \frac{\tau - t_{\theta,\phi}}{\sigma},$$

$t_{\theta,\phi}$ is the difference of the arrival times of particles in two detectors for a shower from the direction (θ, ϕ), and τ is the maximum time difference allowed between two detectors (threshold level). Π_i, the effective area times solid angle times time triggering probability, for each of the three triggering requirements, is given by

$$\Pi_i(N, s, \tau, \sigma) = \int\int A_{N,s}(\theta, \phi) P^2_{\tau,\sigma}(\theta, \phi) \sin\theta\, d\theta\, d\phi. \tag{2}$$

The calculation has been made in bins of $10° \times 10°$ in θ and ϕ. The zenith angle dependence of Π is shown in figure 3. The overlapping of the effective area for the different conditions has been taken into account; figure 3(*a*) is for the M-run and figure 3(*b*) is for the S-run. Each point represents the value for a 10° interval in zenith angle. In order not to confuse the diagram only values for age parameters $s = 1{\cdot}0$ are plotted for size $\lg N = 4{\cdot}5$. It is to be noted that the slope of the zenith angle dependence of Π is independent of the size and age of the shower. The change of Π between $s = 0{\cdot}6$ and $1{\cdot}0$ is less than 10% for the shower size of 10^4 and 80% for the shower size of 3×10^3.

3. Analysis

3.1. Determination of arrival direction

The arrival direction of each shower is calculated by a least-squares fit from the readings of the ten fast timing channels. The 'quality of fit' (δ) is represented (in m^2) by

$$\delta^2 = \sum_{i=1}^{k} \frac{(ct_i - lx_i - my_i - nz_i)^2}{k-2} \tag{3}$$

where x_i, y_i, z_i are the separations of the two detectors in x, y, z directions respectively, t_i is the arrival time difference of particles in channel i; (l, m, n) are directional cosines and k is the number of channels fired. We have selected only showers with $\delta^2 < 1{\cdot}0$.

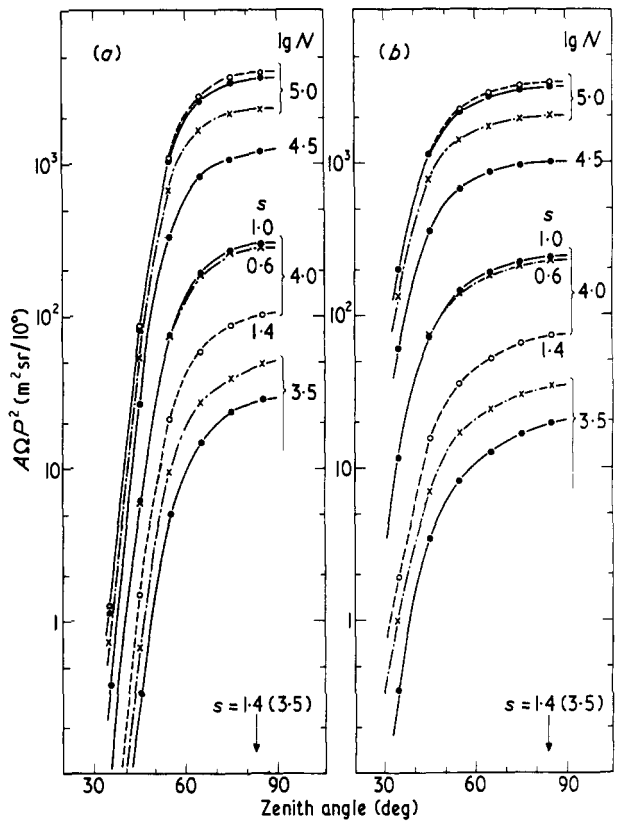

Figure 3. Zenith angle dependence of Π (effective area A times solid angle Ω times triggering efficiency P^2) per 10° in zenith angle. × $s = 0{\cdot}6$; ● $s = 1{\cdot}0$; ○ $s = 1{\cdot}4$.

This criterion has been chosen from the result of Monte Carlo simulations described in appendix 1. The errors in time measurement are due to the arrival time fluctuation of particles in the shower and time fluctuations due to the electronic measuring system. The latter depend on the pulse height of the light collected and become smaller as the number of incident particles or the path length in the scintillator increases. If the fluctuations due to this effect are expressed by a gaussian distribution for each timing channel, its standard deviation σ_ρ for the present apparatus as derived from measurements by van Staa (1968) is approximately

$$\sigma_\rho = \begin{cases} 4{\cdot}0\,\rho^{-0{\cdot}46}\ \text{ns} & \text{for } \rho \leqslant 20 \text{ particles/detector} \\ 1{\cdot}0\ \text{ns} & \text{for } \rho > 20 \text{ particles/detector} \end{cases} \tag{4}$$

where ρ is the smaller one of the pulse heights recorded in the two detectors in units of relativistic particles incident perpendicular to the detector.

The thickness of the shower disc may be expressed by a gaussian distribution. The standard deviation as obtained by Woidneck *et al* (1971) can be approximated by

$$\sigma_t(r, \theta) = (0{\cdot}06r + 2{\cdot}5)\ \text{ns} \qquad (\text{for } r \leqslant 60\,\text{m}), \tag{5}$$

as a function of core distance r, independent of the zenith angle θ up to 45°. Since there

are no measurements available for zenith angles above 45°, we have determined σ_t by a separate run (S-run), which is described in § 4.1.

The total error in time measurement for each channel is,

$$\sigma_{\text{time}} = (\sigma_\rho^2 + \sigma_{t1}^2 + \sigma_{t2}^2)^{1/2} \tag{6}$$

where suffixes 1 and 2 correspond to the two detectors of the combination. We have taken $\sigma_{t1} = 3{\cdot}7$ ns ($r = 20$ m) and $\sigma_{t2} = 2{\cdot}5$ ns to estimate σ_{time} for our triggering condition, since in nearly all cases there are more than two particles in one of the two detectors of each fast timing channel. For $\sigma_\rho = 4$ ns, we get $\sigma_{\text{time}} = 6$ ns. Figure 4 shows the angular resolution for a $\sigma_{\text{time}} = 6$ ns, chosen independent of zenith angle, calculated by Monte Carlo methods, details of which are outlined in appendix 1. The chain curve represents the angular resolution of the previous array (Böhm *et al* 1971). The improvement in angular resolution of the present configuration is clearly to be seen.

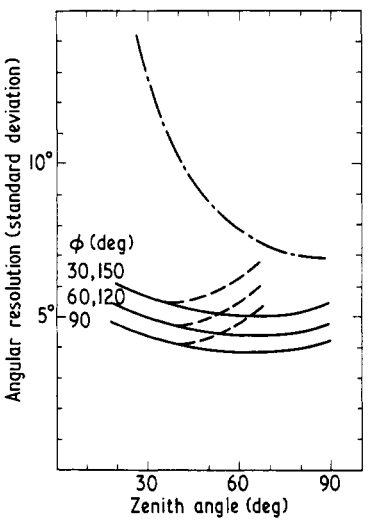

Figure 4. Zenith angle dependence of the angular resolution.

3.2. Determination of shower size

For the size determination there are 9 horizontal detectors (H1–H9) and 16 vertical detectors (V1–V16) of 1 m^2 each. Due to the increase of the path length and the decrease of the effective area with zenith angle, the fluctuations in the scintillator response are much larger for the vertical detectors than for the horizontal ones. Therefore the shower size has been calculated from the response of the horizontal detectors only and the vertical detectors have been used to check the size determination and to exclude large showers ($N > 10^5$).

The method of calculation has been the following. The density of the nine detectors has been fitted to the NKG function with $s = 1{\cdot}0$ in each point of a grid of 18×18 points with two kinds of spacing, 2 m and 5 m. In each point the size and the mean square deviation of the fit

$$\epsilon_H^2 = \sum_{i=1}^{k} \frac{(n_i - m_i)^2}{k-3}$$

have been calculated (n_i and m_i are observed and expected densities and k is the number of detectors fired). The area covered by the grids is large enough for showers smaller than 10^5. We have chosen the grid point of the minimal ϵ_H as the core position. If there were two points of the minimal ϵ_H within a difference of 0·1, we took that grid point as core position which had the smaller ϵ_{H+V}, determined from both horizontal and vertical detectors. The uncertainty introduced by this method has been estimated from a simulation of the detection process by Monte Carlo methods as described in appendix 1.

The calculated shower size N_c deviates from the actual shower size N, the amount of deviation depends on s, θ and ϕ. The shower size N_c is corrected with the following empirical equation, obtained by the Monte Carlo simulation hereafter called observed shower size N_0:

$$\lg N_0(\theta, \phi) = \lg N_c + 0{\cdot}0032\,\theta + 0{\cdot}0020\,\phi - 0{\cdot}426 \qquad (3{\cdot}5 < \lg N < 5{\cdot}0; s = 1). \tag{7}$$

It is important to note that even N_0 differs from N because of the errors in the determination of N_0 in connection with the steepness of the shower size spectrum. Taking into account the triggering probability times effective area Π given in § 2.2, the relation between N and N_0 has been calculated for various combinations of the slope γ of the size spectrum and the shower age s. In figure 5 three examples are shown for the M-run. The flux of showers observed with size N_0 is a composite of various shower sizes N. The contribution of different N is independent of the zenith angle.

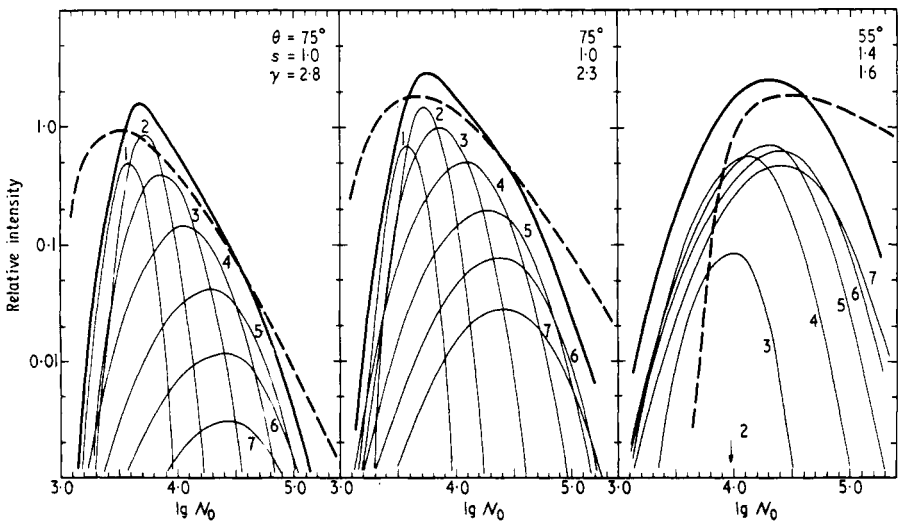

Figure 5. Examples of the deviation of the observed size (N_0) distribution (full curves) from the expected size (N) distribution (broken curves) due to the uncertainty of the size determination. The numbers 1–7 are the contributions from each size interval in logarithmic scale 1:3·05–3·35; 2:3·35–3·65; 3:3·65–3·95; 4:3·95–4·25; 5:4·25–4·55; 6:4·55–4·85; 7:4·85–5·15.

Since we have fitted all showers to the structure function of $s = 1{\cdot}0$, the shower size N_c is overestimated, if the age of the shower is smaller than 1·0, and *vice versa*. The amount of error due to the change of s is less than 15% for $\Delta s = 0{\cdot}4$ between $\lg N = 3{\cdot}5$ and 4·5. Since the size determination of the present configuration is not accurate enough for large showers, events with particles in more than 4 detectors of V10–V16 have been

omitted. We have restricted ourselves to shower sizes ($\lg N_0$) smaller than 4·85 for analysis, in order to assure a reliable size determination with the above method of analysis.

4. Detailed study of the EAS between 35° and 65°

The zenith angle distribution of EAS is shifted to larger zenith angles because of the error in angle determination and the steep zenith angle distribution of EAS. The large absolute flux of EAS compared to HAS gives a contribution of EAS with $\theta < 60°$ to $\theta > 70°$ even for an angular resolution of 5°. The proportion of EAS in which the zenith angle is overestimated depends on the thickness of the shower disc and the attenuation mean free path Λ_{att} of EAS. In the following we first investigate the thickness of the shower disc for zenith angles between 45° and 60° and determine Λ_{att} by means of the zenith angle distribution of EAS up to 65°.

4.1. Thickness of the shower disc

The distribution of $\Delta d = (ct_i - lx_i - my_i - nz_i)$ in equation (3) of each fast timing channel reflects the arrival time distribution of particles in the shower front. Figure 6(*a*) shows the standard deviation σ_{time} of the distribution ($\Delta d/c$) of the fast timing channel (H2–H5) as a function of zenith angle. This channel is almost free from the triggering requirement.

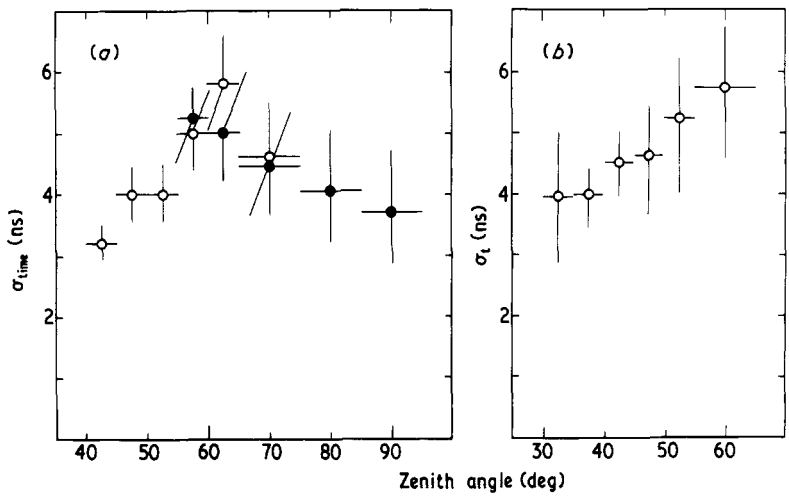

Figure 6. Zenith angle dependence of (*a*) σ_{time} and (*b*) σ_t.

But since we have used only showers with $\delta^2 < 1{\cdot}0$ (in the determination of the arrival direction, the channel H2–H5 has been used) and since the effect of σ_ρ on σ_{time} has not been excluded, this σ_{time} does not express the thickness of the shower disc without any bias. However, it is clear from the figure that σ_{time} increases up to 60°, and decreases above 60° showing that showers at great depths are young showers.

In order to know the actual thickness of the shower disc (σ_t in standard deviations) between 35° and 65°, the information from the six vertical fast timing channels has been

used. The result is shown in figure 6(*b*). Using these values, the accuracy of zenith angle determination for the vertical EAS is revised (broken curves in figure 4).

4.2. Attenuation mean free path of EAS

The attenuation mean free path Λ_{att} of EAS has been measured by many groups up to 50° The values lie between 100 g cm^{-2} and 120 g cm^{-2} for shower sizes around 10^5 at sea level (a summary is given by Hayakawa 1969). However, there are no data available for sizes of about 10^4, $\theta > 50°$. In figure 7 the experimental results of the S-run are shown.

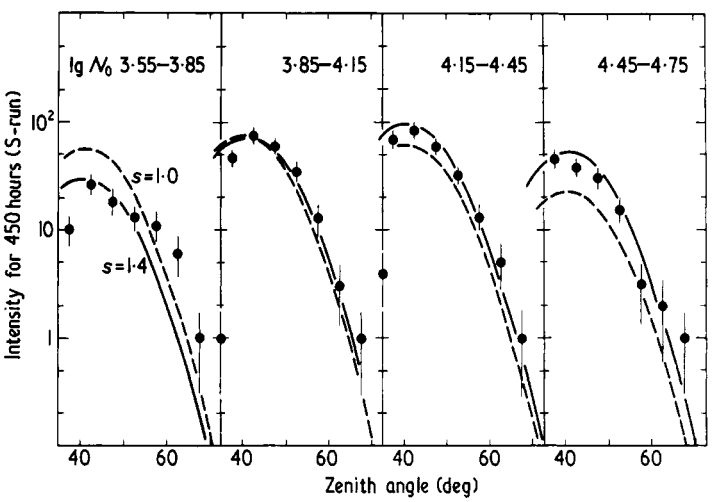

Figure 7. Expected and measured zenith angle distribution of EAS between 35° and 70° for four size intervals (S-run). Full curve: $s = 1{\cdot}4$; broken curve: $s = 1{\cdot}0$.

The zenith angle distribution between 35° and 65° is plotted for four different size regions. The expected curves have been calculated assuming the integral size spectrum at zenith angle θ to be

$$I(\theta, \geqslant N) = I_0 \left(\frac{N}{10^5}\right)^{-\gamma} \exp\left(-\frac{1030(\sec\theta - 1)}{\Lambda_{att}}\right) \tag{8}$$

with the following parameters: $\Lambda_{att} = 100$, 110 and 120 g cm^{-2}, $\gamma = 1{\cdot}7$. The effective area times triggering probability Π has been used for three different ages ($s = 1{\cdot}0$, 1·2 and 1·4). Details of the calculation are described in appendix 2. The change of thickness of the shower disc with zenith angle obtained in the preceding section has been taken into account. For $s = 1{\cdot}4$ we get the best agreement with the experimental points in all size intervals. The slope of the angular distribution does not change with Λ_{att} between 100–120 g cm^{-2} because of the limited angular resolution, but the absolute intensity depends much on Λ_{att}. If we take the intensity $I_0 = (1{\cdot}4 \pm 0{\cdot}3) \times 10^{-10}$ cm^{-2} s^{-1} sr^{-1} (Miura and Hasegawa 1962, Khristiansen *et al* 1965), the agreement is obtained for $\Lambda_{att} = (120 \pm 5)$ g cm^{-2}. Figure 7 shows examples for $\Lambda_{att} = 120$ g cm^{-2}, $s = 1{\cdot}0$ and 1·4. It is to be noted that a deviation from expectations as measured by Catz *et al* (1971) is not observed between 50° and 60°.

5. Results

5.1. Zenith angle distribution of HAS

The observed zenith angle distribution for the M-run is shown in figure 8 for four size intervals. Due to the errors in angle determination (figure 4), there are showers with zenith angles larger than 90°. The expected distribution is calculated from the size spectrum of muon bremsstrahlung given by Király *et al* (1971) with an enhancement factor of muons from pion decay given by Maeda (1970).

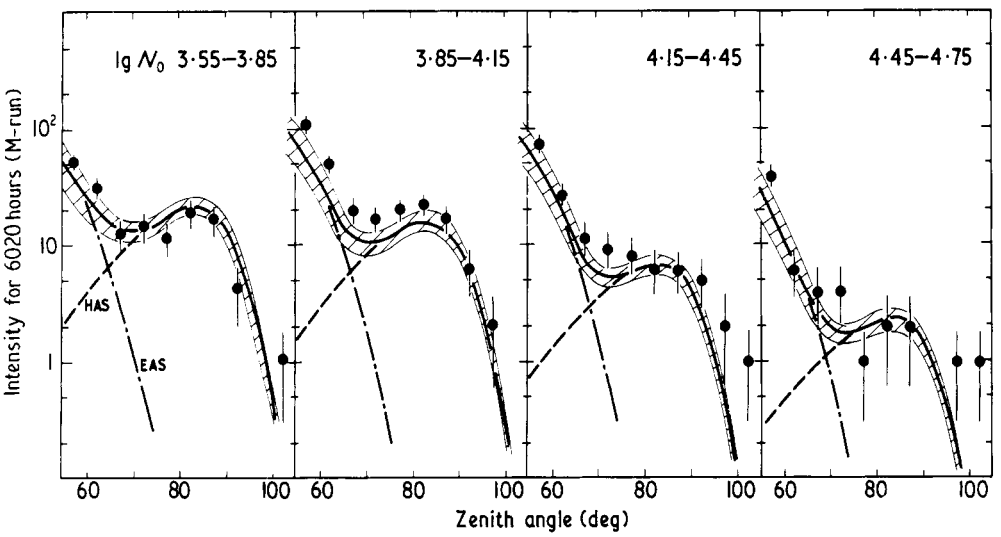

Figure 8. Expected and measured zenith angle distribution of HAS for four size intervals (M-run).

Because of the steepness of the size spectrum of HAS and the age dependence of Π, the observed HAS are most likely to be at the maximum development and we have used the value of Π ($s = 1{\cdot}0$) for HAS and the values of $I_0 = (1{\cdot}4 \pm 0{\cdot}3) \times 10^{-10}$ cm^{-2} s^{-1} sr^{-1}, $\Lambda_{att} = 120$ g cm^{-2} and Π for $s = 1{\cdot}4$ for EAS based on the results of the preceding section. The method of calculation is described in appendix 2. The uncertainty in zenith angle determination given in figure 4 has been taken into account. The errors on the experimental points are statistical ones only. Additional errors result from uncertainties in the calculation of Π and in size determination estimated to be $\pm 20\%$ for HAS and $\pm 40\%$ for EAS, are shown as shaded areas in figure 8.

The calculated proportion of the EAS above 70° is 0·2–6·4 % depending on shower size as listed in table 2. This is consistent with the estimate from the result of the refined Monte Carlo simulation described in appendix 1 (C-series).

Table 2. Proportion of EAS contamination to HAS above 70°

lg N_0	3·55–3·85	3·85–4·15	4·15–4·45	4·45–4·75
Proportion (%)	0·3–1·1	0·8–3·4	1·2–4·2	1·6–6·4

5.2. Size spectrum of HAS

The integral size spectrum of showers of zenith angles larger than 70° is shown in figure 9 by large full circles. The large open circles represent our previous result (Böhm *et al* 1971), they coincide with the new result within experimental uncertainties. The

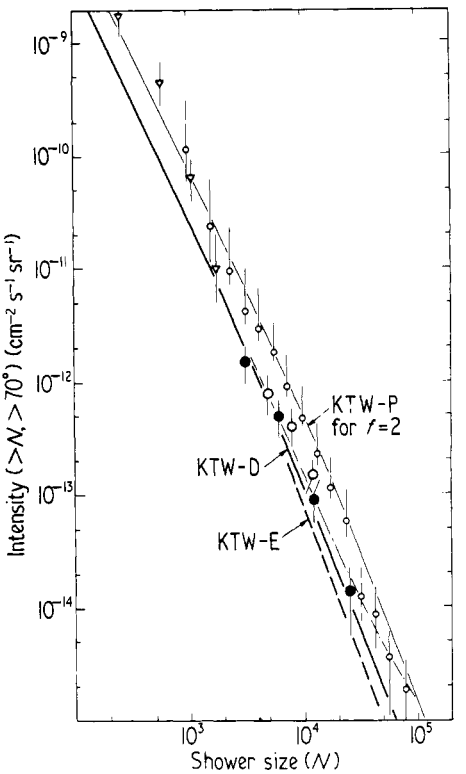

Figure 9. Integral size spectrum of HAS above 70°. ♦ Present experiment; ◊ Kiel results (1971); ◊ Tokyo (INS) results (1969); ▽ Durham results (1971).

error bars given are the sum of statistical errors and the additional errors mentioned in the previous section. The systematic deviations between N and N_0 as shown in figure 5 have been taken into account. The integral size spectrum for $\theta \geqslant 70°$ is

$$I(\geqslant N, \geqslant 70°) = (1{\cdot}3 \pm 0{\cdot}4) \times 10^{-13} \left(\frac{N}{10^4}\right)^{-2{\cdot}4 \pm 0{\cdot}2} \text{ cm}^{-2}\,\text{s}^{-1}\,\text{sr}^{-1} \qquad (9)$$

in the range $3{\cdot}5 \leqslant \lg N \leqslant 4{\cdot}5$. For comparison the expected size spectrum for muon bremsstrahlung as calculated by Király *et al* (1971) is shown in figure 9 by full (KTW–D) and broken (KTW–E) lines. The present result is in good agreement with KTW–D and coincides also with KTW–E within the limit of the experimental uncertainties. A detailed discussion will be made in § 6.

5.3. Muons in inclined EAS and in HAS

A preliminary check on the muon content in inclined EAS and in HAS has been made by

using the shielded detector (M1) (see figure 1). The ratio of muons to electrons ρ_μ/ρ_e has been determined by dividing the number of muons observed in M1 by the average of the number of particles observed in V1, V2, V3 and V4. The ratio is shown in figure 10

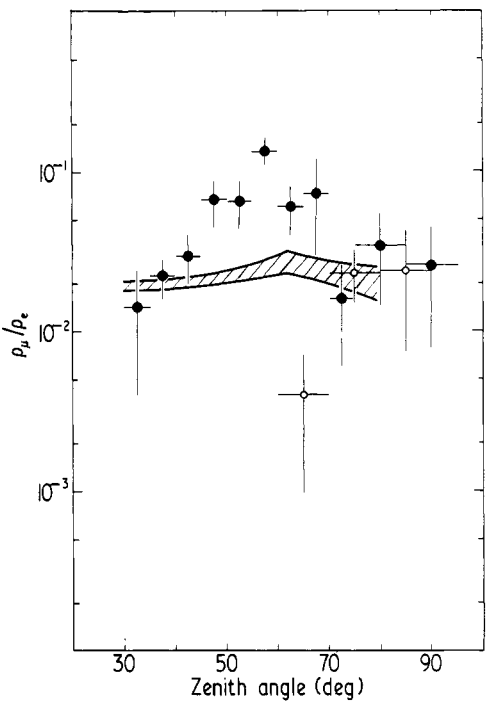

Figure 10. Zenith angle dependence of the ratio of densities of muons to electrons for $N > 10^5$. -●- Present experiment; -⊹- Tokyo (INS) results (1969); shaded area gives the Paris results (1971).

as a function of zenith angle. The arrival time distribution of muons relative to shower particles in V1 is shown in figure 11 for five zenith angle intervals. Positive values indicate that the muons arrive at the observation level earlier than any particle in V1. There is no time information if no particle hits V1, even if a muon is observed in M1.

7 muons in 204 showers for zenith angles above 70° have been observed. The rate of spurious coincidences of muons is at most 1 per 10^4 showers, because the gain of the photomultiplier is reduced by a factor of 80 for 22 μs by a dynode gating circuit (Roose 1965) within 1 μs after the coincidence signal. Since the effective area covers on the average 400 m^2, the probability that the parent muon of the HAS hits the detector is about 400 m^2/0·25 m^2 corresponding to about 1 per 1600 showers for HAS.

The present results can be summarized as follows: (i) The ratio ρ_μ/ρ_e has a maximum at around 55°–60° and then decreases. (ii) ρ_μ/ρ_e is more than 0·01 and almost constant above 70°. The muons in these showers are not trivial. (iii) The arrival times of muons are the same as those of electrons in all zenith angle regions. The spread in the distribution increases until 60°, and has the tendency to become constant or even to decrease above 60°. (iv) Four burst events are observed within 1157 picked up showers of $\theta \geqslant 30°$. They are listed in table 3.

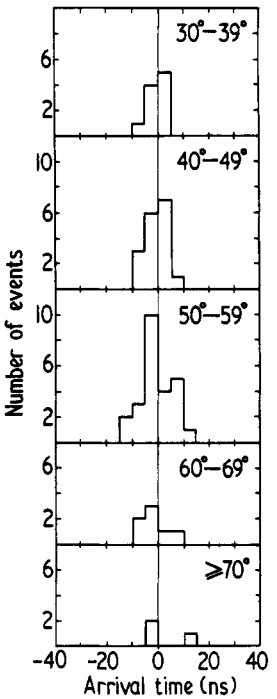

Figure 11. Arrival time distribution of muons in M1 relative to shower particles in V1.

Table 3. List of bursts associated with EAS and HAS

Event number	Arrival direction		Size		Burst size (particles)		Arrival time relative to V1 (ns)
	zenith	azimuth	lg N_0	s	observed	corrected	
183482	57	114	3·9	>1·4	21	11	—
297090	86	43	4·5	~0·6	66	5–10	−0·4
301083	64	121	4·5	>1·4	27	12	+2·9
721066	63	105	3·9	>1·4	140	64	+3·8

6. Discussion

The observed zenith angle distribution is consistent with the distribution for muons of pionic (and/or to some extent of kaonic) origin within experimental uncertainties for observed shower sizes N_0 between 4×10^3 and $6{\cdot}3 \times 10^4$. The corrected sizes N correspond on the average to about $2{\cdot}5 \times 10^3$ and $3{\cdot}1 \times 10^4$ respectively.

The size spectrum is in good agreement with that due to muon bremsstrahlung (KTW–D in figure 9) calculated by Király *et al* (1971), extrapolating the muon spectrum D–70 with the same exponent (~2·6) to energies larger than 10^{13} eV. This muon spectrum D–70 has been derived by Király and Wolfendale (1970) from the depth–intensity relation of muons with the assumption that the value b, the coefficient in the energy loss formula of muons, is 4·18 and $4{\cdot}36 \times 10^{-6}$ g^{-1} cm^2 at $E = 10^{12}$ and 10^{13} eV respectively. These values are larger than those usually accepted. In figure 9 the experimental

results from the Tokyo (INS) group (Nagano *et al* 1971) and the Durham group (Király *et al* 1971) are also shown. The uncertainties due to the change of the effective area with the age parameter have been added to the error bars of the Tokyo (INS) data. Since a correction for the errors in the shower size determination has not been made in the Tokyo (INS) measurements, their results should be compared with the calculation for $f = 2$ (thin line) (f being the uncertainty factor in the size determination). The agreement with the expectation (KTW–D) is also quite good.

The integral energy spectrum of muons calculated from the observed size spectrum derived with the same method as Király *et al* (1971) is shown in figure 12 by the shaded area. In the same figure some experimental results and calculated spectra are shown

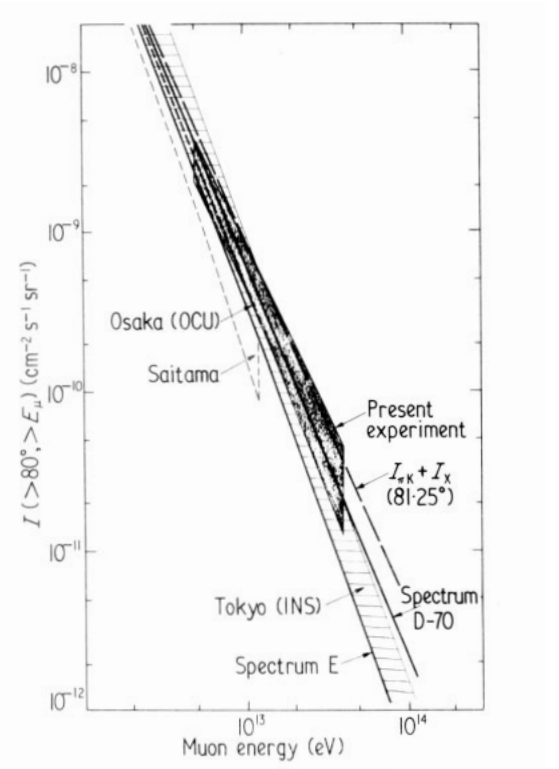

Figure 12. Integral energy spectrum of muons above 80°.

for comparison. All spectra except $(I_{\pi K} + I_X)$ are converted from the results obtained at various zenith angles to those of $\theta \geqslant 80°$ with the muon enhancement factor given by Maeda (1970). The energy of the muons has not been determined directly in these energy regions. The spectra have been obtained by measuring the energy transferred to bursts or the size of bursts produced by muons. The Saitama group has measured the energy transferred to bursts produced in lead with multiple layers of x ray film (Mizutani *et al* 1971), the Osaka (OCU) group has measured the size spectrum of bursts in rock with two layers of scintillators (Chin *et al* 1971), the Tokyo (INS) (Nagano *et al* 1971) and the present results have been obtained from the size spectrum of HAS with a scintillation detector array. Below 10^{13} eV all experiments are in agreement with spectrum E within experimental uncertainties, but not all with D–70. The spectrum

E derived from the primary spectrum by Király and Wolfendale (1970) agrees with that derived from the depth–intensity relation of muons if b is $3{\cdot}6 \times 10^{-6}$ g^{-1} cm^2; this value is generally accepted from the comparison between the muon energy spectrum directly measured by magnetic spectrometers and the depth–intensity relation of muons (for example, see Menon and Ramana Murthy 1967). The spectrum E fits to the various experiments and hence it can be considered to represent the muon spectrum of pionic origin better than the spectrum D–70 up to 10^{13} eV. Assuming that the spectrum E holds for the muon spectrum of pion decay further above 10^{13} eV, the angular distributions thus obtained are compared with the present results, represented by full curves in four size intervals in figure 13. The expected curves seem to be systematically lower than the experimental points for lg $N_0 \geqslant 3{\cdot}85$.

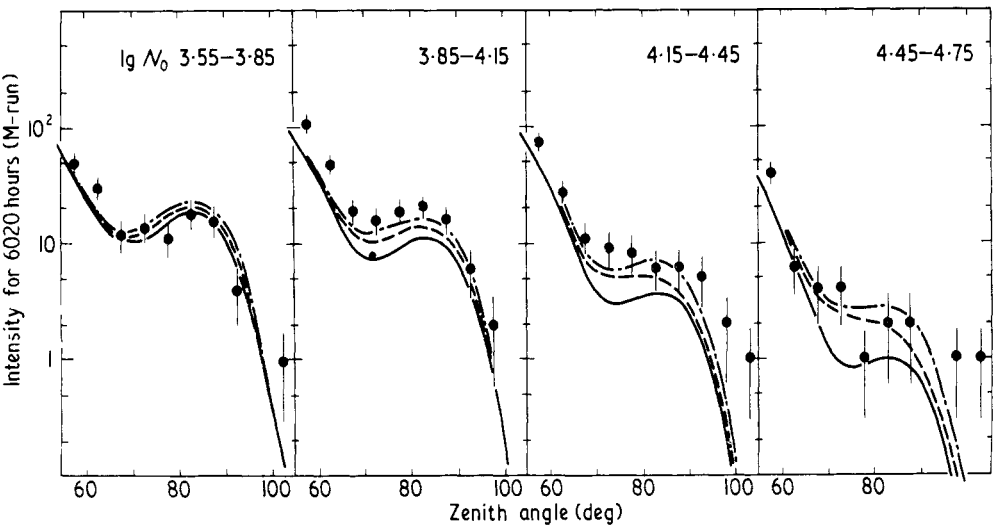

Figure 13. Expected and measured zenith angle distribution with an isotropic component or an attenuation type component, each of them added to the muon component from pion decay.

Assuming these systematic differences to be real we can think of three possibilities of explanation: (i) an additional process of muon production different from pion (and/or kaon) decay; (ii) shower production by other particles than muons; or (iii) larger interaction cross section of muons in the energy region above 10^{13} eV than the one extrapolated from the accelerator energy region.

In the following we first discuss the possibilities (i) and (ii), assuming that the above stated systematic difference were real. The typical zenith angle distribution of such components for (i) would be isotropic, examples are muons from the intermediate boson W (Bjorken *et al* 1969), muons decayed directly from ϕ of aleph decay proposed by Koshiba *et al* (1967) or muons from X process discussed by Bergeson *et al* (1967). For (ii), an exponential distribution depending on sec θ with the attenuation mean free path Λ would be expected, for example from quarks (Gell-Mann 1964, Zweig 1964) or heavy integer-charged triplets (for example, see Lee 1965). We assume for simplicity that the expected size spectrum of these particles has the same exponent as the primary spectrum. This is true if the characteristics of production and interaction of the assumed particles are

independent of energy. With this assumption the integral size spectra of such components observed at sea level with zenith angle θ would be

$$I_{\rm iso}(\geqslant N,\theta) = I^0_{\rm iso}\left(\frac{N}{10^4}\right)^{-\gamma} \tag{10}$$

and

$$I_{\rm att}(\geqslant N,\theta) = I^0_{\rm att}\left(\frac{N}{10^4}\right)^{-\gamma} \exp\left(-\frac{1030(\sec\theta-1)}{\Lambda}\right) \tag{11}$$

where $I^0_{\rm iso}$ and $I^0_{\rm att}$ are the vertical intensities at $N \geqslant 10^4$. The expected curves fit to the results of the present experiment, when the intensities of these components are taken to be the same as for muons at $\theta = 70°$ for a size of 10^4. That is, the vertical intensities are $I^0_{\rm iso} = 7{\cdot}5\times10^{-14}$ and $I^0_{\rm att} = 1{\cdot}3\times10^{-13}$ cm^{-2} s^{-1} sr^{-1}. The chain curves in figure 13 are expected for an isotropic component, the broken curves for absorption of $\Lambda = 5000$ g cm^{-2}, added each of them to the sec θ distribution of muons from spectrum E. Here γ is taken to be 1·7. The size spectrum expected from muons of spectrum E together with an isotropic component or an attenuation type component is flatter than the spectrum E as shown by chain curves in figure 9. The slope is about 2·2, in agreement with the present results within experimental uncertainties. In order to be compatible with our results the maximal vertical intensities of these components for $N \geqslant 10^4$ are $I^0_{\rm iso} = 1{\cdot}1\times10^{-13}$ and $I^0_{\rm att} = 1{\cdot}9\times10^{-13}$ cm^{-2} s^{-1} sr^{-1}. It is to be noted that this flux of an isotropic component is in agreement with the muon spectrum through W derived by Carlson *et al* (1971) ($I_{\pi K}+I_X$) or with the spectrum for muons directly from ϕ of aleph decay (Koshiba 1972, private communication) within a factor of 1·5. The energy of a heavy mass particle which produces a shower of size 10^4 depends on its interaction characteristics. If we use the inelasticity $K_{\rm H} = k_{\rm N}m_{\rm N}/M_{\rm H}$ ($k_{\rm N}$, $m_{\rm N}$ and $K_{\rm H}, M_{\rm H}$ are inelasticity and mass of the nucleon and heavy mass particles respectively) following Adair and Price (1966), the shower size 10^4 corresponds to about 10^{14} eV for a mass $M_{\rm H} = 10$ GeV. The upper limit of the flux given here for heavy mass particles which can produce a shower of energy about 2×10^{13} eV is about two orders of magnitude smaller than the upper limit set by various search experiments (for example, Faissner *et al* 1970).

The increase of the interaction cross section of muons at high energies is the possibility (iii), to explain the systematically higher rate of events. The electromagnetic interaction of muons can be calculated from quantum electrodynamics (QED). But even if it is believed that QED still holds above 10^{12} eV, the calculation now gives slightly different results. For example, Erlykin (1965) has calculated a value 20% larger than the generally accepted one, which recently has been supported by Wright (1973), favouring the b value used in deriving spectrum D–70. However, more ambiguity lies in the cross section of the muon–nucleon interaction in the high energy region. If it increases to several times 10^{-29} cm^2 for muon energy above 10^{13} eV, we may expect as many nuclear cascade showers as purely electromagnetic cascade showers due to bremsstrahlung (Nagano *et al* 1971). Such showers can in principle be distinguished from electromagnetic ones due to the abundance of muons and hadrons in the showers.

We have observed 7 muons within 204 showers for zenith angles above 70°. This proportion agrees with 9 muons within 35 showers observed by the Tokyo (INS) group (Nagano *et al* 1971), if we take into account the difference in the effective area of the muon detectors in the two experiments ($\sim$0·25 m^2 Kiel and $\sim$3 m^2 Tokyo (INS)). The ratio ρ_μ/ρ_e is larger than 0·01 (figure 10). The value is about one order of magnitude

higher than would be expected from a purely electromagnetic cascade shower of muon bremsstrahlung. However, there remains the possibility that these muons are remnant muons which have been produced at the top of the atmosphere during the development of the EAS (Nagano *et al* 1971) and not in the HAS or are muons in a shower with zenith angle below 65°, the angle of which has been overestimated due to the error of the zenith angle determination. We will refer to muons produced in HAS as μ_H and those produced in EAS as μ_E. These two kinds of muons (μ_H and μ_E) may be distinguished from each other by the following methods: (*a*) the zenith angle dependence of ρ_μ/ρ_e; (*b*) their arrival time distribution and its zenith angle dependence; and (*c*) their lateral distribution. The differences in behaviour between μ_H and μ_E are compared in table 4.

Table 4. Comparison of various distributions for μ_H and μ_E

	μ_H	μ_E
(*a*) Zenith angle dependence of ρ_μ/ρ_e	independent of zenith angle	increases with zenith angle
(*b*) Arrival time distribution	the same as for EAS at the maximum development	broader distribution than for μ_H
(*c*) Lateral distribution	the same as for EAS at the maximum development	broad lateral distribution over a few hundred m from the core of HAS

The present results (ii) and (iii) in § 5.3 favour the theory that muons are produced during the development of HAS, but better statistics are required for a confirmation.

Besides single muons, four burst events have been observed as shown in table 3, which can be related to the hadron component in HAS. Three of them below 65° may be produced by high energy muons in the concrete. Such a frequency can be explained by muon bursts associated with EAS (Nagano 1964, unpublished). In the case of the event 297090, the shower seems to be very young ($s \sim 0{\cdot}6$) and the zenith angle of the shower is very large and hence the burst is likely to be a tail of a burst produced by a hadron ($\geqslant 200$ GeV) in a nuclear cascade. But the possibility of it being produced by a high energy photon or electron in a purely electromagnetic cascade shower cannot be excluded.

We suppose that with the new detector M2 in figure 1 the distinction between μ_H and μ_E will be possible to detect with the methods described above in table 4. If we observe bursts with this detector, they are more likely to be due to hadrons than high energy photons or electrons, because low energy photons and electrons in the tail of a high energy electromagnetic cascade which pass the first shielding are scattered away and are not observed as a burst after the second shielding (see figure 1).

It should be added that if there are heavy mass particles with the flux stated before, muons in HAS will be explained without invoking any increase of the muon–nucleon interaction cross section. In such a case there may be a strong size dependence of muon content in HAS.

7. Conclusions

The zenith angle distribution of EAS has a constant attenuation mean free path Λ_{att} up to 60°–65°. Λ_{att} is 110–120 g cm^{-2} if the vertical intensity of $N \geqslant 10^5$ is taken to be

$(1{\cdot}4 \pm 0{\cdot}3) \times 10^{-10}$ cm^{-2} s^{-1} sr^{-1}. The average shower age increases with zenith angle up to 60°–65° and again decreases (see figure 6(*a*) and figure 10), indicating that the EAS observed above 70° are not produced directly by primary particles but by penetrating secondaries. From the zenith angle distribution of EAS and HAS the proportion of contamination of EAS to HAS above 70° is estimated to be 0·3–6·4 % depending on shower size and hence the contribution of EAS to the size spectrum and the muon content of HAS is negligible.

Both the size spectrum and the zenith angle distribution of HAS are in good agreement with those expected from the muon energy spectrum D–70 (Király and Wolfendale 1970) and the muon enhancement factor for pionic origin (Maeda 1970) for the shower size N between $2{\cdot}5 \times 10^3$ and $3{\cdot}1 \times 10^4$. That is, high energy cosmic ray muons can be considered to be produced mainly through pion (and/or to some extent through kaon) decay up to muon energies of 5×10^{13} eV. If we adopt spectrum E, which gives a better agreement with various experiments up to 10^{13} eV, the present experimental results are compatible with the additional flux of an isotropic component from muons produced directly or through short-lived particles of $I^0_{\rm iso} = 1{\cdot}1 \times 10^{-13}$ cm^{-2} s^{-1} sr^{-1}, or with the additional flux of a component with attenuation mean free path larger than 5000 g cm^{-2} from heavy mass particles of $I^0_{\rm att} = 1{\cdot}9 \times 10^{-13}$ cm^{-2} s^{-1} sr^{-1}.

The number of muons associated with HAS is about one order of magnitude larger than expected in cascade showers from muon bremsstrahlung. Since there are some indications that these muons are produced during the development of HAS, this experiment will be continued further with a new muon detector of 2·25 m^2. Here special attention will be paid to distinguish the muons produced in HAS from the remnant muons in EAS.

Acknowledgments

The authors would like to thank Professor E Bagge for his encouragement. Professor J Trümper started this experiment and took part in the first stage of development. We would like to express our sincere thanks to him for continuous interest and valuable discussions. We have to thank Dipl. Phys. R van Staa, who has been involved in the early stage of this experiment, Dipl. Phys. E Kendziorra and Dipl. Phys. H P Hoffmann for their contribution to the experiment. We are indebted to Ing. K Sauerland for his help in the construction and running of the apparatus.

We are also grateful to Professor A W Wolfendale and Dr P Király for useful discussions on the size spectrum of HAS.

M Nagano wishes to thank Professor K Suga and Professor S Mikamo for useful discussions and correspondence and the Alexander von Humboldt-Stiftung and the Nishina Memorial Foundation for supporting his study in Kiel.

This work has been supported by the Deutsche Forschungsgemeinschaft under grant Tr. 11/1.

Appendix 1. Check and calibration of the analysis method by simulated showers

In order to know the amount of uncertainties introduced by the analysis procedure described in § 3, we have simulated the detection of showers by Monte Carlo methods with the following three series of conditions.

(*A-series*). (i) Lateral distribution: NKG function (s = 0·6, 1·0 and 1·4); (ii) fluctuations of the density in each detector: poissonian distribution; (iii) core position: randomly over an area as given below; and (iv) fluctuations of fast timing channels: a gaussian distribution with a standard deviation σ_{time} of 6 ns.

The area has been chosen for every size individually to have a triggering efficiency of about 15–20%. The simulations have been made for various combinations of zenith angles, azimuth angles, shower sizes and shower ages. The number of showers simulated in each run has been 600, that is, 100–120 showers have triggered and have been recorded in the same way as real showers in each run. The simulated showers have been analysed with the procedure described in § 3.

The error in zenith angle determination depends on the arrival direction and has been found to be within 5° between 40° and 90° as shown in figure 4. The average shower size deviates from the input shower size, and the amount of deviation depends on θ, ϕ and s. The calculated shower size is corrected by the empirical formula (equation (7)) derived from this simulation.

(*B-series*). In order to calculate the relation between the error in timing σ_{time} and in zenith angle determination σ_{ZA}, the simulations have been made in a similar way by varying the values of condition (iv) of series A. The relation found can be expressed by

$$\sigma_{\text{ZA}} = 0{\cdot}62\,(\sigma_{\text{time}} - 6{\cdot}0) + \sigma_{\theta,\phi}\,(6{\cdot}0).$$

σ_{ZA} is in degrees where $\sigma_{\theta,\phi}(6{\cdot}0)$ is the standard deviation for the arrival direction (θ, ϕ) in the case of σ_{time} = 6·0 ns, shown in figure 4, and σ_{time} in ns. The change of error in size determination is within 10% for a change of σ_{time} from 6 to 10 ns.

(*C-series*). It is well known that the tail of the time distribution of the shower disc is better fitted with an exponential form than with a gaussian form. Since this tail is of importance in knowing the proportion of vertical showers whose zenith angles are analysed to be larger than 70°, a simulation has been performed using the following condition instead of (iv): delay time distribution of shower particles

$$w(t_{\text{d}}) = \frac{1}{\tau}\exp\left(-\frac{t_{\text{d}}}{\tau}\right) \mathrm{d}t_{\text{d}}.$$

If the particle density in each detector is given, the delay time of the first particle in each detector is obtained by simulating the delay time of each particle according to the distribution given above. The signals for each channel have been combined and then the delay time has been corrected using equation (4). The simulations have been made for two values of τ: (*a*) 5 ns which fits to the results of Woidneck *et al* (1971); and (*b*) 10 ns in order to check the τ dependence. 2000 showers have been simulated in each case. The results are listed in table 5.

Table 5. Result of the Monte Carlo simulations (C-series). P means proportion of selected showers ($\delta^2 < 1{\cdot}0$) to all showers

τ(ns)	P	σ_{ZA}	$\theta \geqslant 65°$	$\theta \geqslant 70°$
5	94% of all showers	4·1° up to 65°	(2·0 ± 0·8)% of selected showers	(0·66 ± 0·46)% of selected showers
10	72% of all showers	6·0° up to 65°	(7·1 ± 1·5)% of selected showers	(2·2 ± 0·85)% of selected showers

The various proportions in the table coincide with those of the simulation made in series A in the case of $\tau = 5$ ns. This means the extreme fluctuations are suppressed by using more than 7 fast timing channels and the selection criterion $\delta^2 < 1{\cdot}0$, which has been used in the present analysis.

Appendix 2. Calculation of the expected zenith angle distribution

Since there are uncertainties in the size (σ_N), zenith and azimuth angle (σ) determination, the flux of showers with observed angle (θ_0, ϕ_0) is a mixture of showers of various sizes and angles. In the following, we calculate the expected zenith angle distribution for a restricted size region, taking into account the uncertainties in size and angle determination. Since 60% of all showers are observed with azimuth angles between 60° and 120°, we use in the following the value of σ_{ZA} for $\phi = 60°$ and 120° for all θ (figure 4). The method of calculation is the same for EAS and HAS.

Let us assume that the intensity of showers of size N_i in ΔN for constant zenith angle interval θ_k in $\Delta\theta$ is $\Delta I(N_i, \theta_k)$. Some part of them (P_{ij}) is determined to be of size N_j in ΔN due to the uncertainty of size determination. P_{ij} depends not only on σ_N, but also on the effective area times triggering efficiency Π and the slope of the size spectrum γ. Though Π is a function of N, s, τ, σ, and θ as shown in equation (2), P_{ij} is almost independent of θ, as far as s, τ, and γ are constants, since it comes out that the slope of the zenith

Table 6. Examples of P_{ij} (%)

lg N \ lg N_0	<3·25	3·25–3·55	3·55–3·85	3·85–4·15	4·15–4·45	4·45–4·75	>4·75
($\theta = 75°$, $s = 1{\cdot}0$, $\gamma = 2{\cdot}8$)							
3·05–3·35	0·5	54·4	45·0	0·1	0·0	0·0	0·0
3·35–3·65	0·0	12·8	79·3	7·9	0·0	0·0	0·0
3·65–3·95	0·0	7·0	48·9	39·4	4·6	0·1	0·0
3·95–4·25	0·2	4·0	22·7	44·1	25·1	3·6	0·3
4·25–4·55	0·2	2·3	12·1	29·2	37·8	16·1	2·3
4·55–4·85	0·2	1·7	8·8	23·2	35·1	24·5	6·5
>4·85	0·1	1·2	7·1	21·0	33·7	27·3	9·6
($\theta = 75°$, $s = 1{\cdot}0$, $\gamma = 2{\cdot}3$)							
3·05–3·35	0·5	54·5	44·9	0·1	0·0	0·0	0·0
3·35–3·65	0·1	12·1	78·6	9·2	0·0	0·0	0·0
3·65–3·95	0·1	6·7	47·7	40·5	5·0	0·0	0·0
3·95–4·25	0·2	3·9	22·1	43·4	26·2	4·0	0·1
4·25–4·55	0·2	2·3	12·0	29·0	37·8	16·3	2·4
4·55–4·85	0·2	1·7	8·7	23·1	35·0	24·7	6·6
>4·85	0·1	1·2	7·1	21·0	33·7	27·3	1·6
($\theta = 55°$, $s = 1{\cdot}4$, $\gamma = 1{\cdot}6$)							
3·05–3·35	0·0	0·0	0·0	0·0	0·0	0·0	0·0
3·35–3·65	0·0	0·0	0·0	0·0	0·0	0·0	0·0
3·65–3·95	0·4	9·7	45·0	41·0	3·9	0·0	0·0
3·95–4·25	0·6	7·1	28·0	43·0	19·0	2·2	0·1
4·25–4·55	0·5	4·1	16·9	33·2	33·6	10·5	1·2
4·55–4·85	0·4	2·9	12·4	27·2	35·1	18·2	3·8
>4·85	0·2	2·3	10·9	25·9	34·1	20·9	5·2

angle dependence of Π is independent of size. By using the σ_N obtained from the Monte Carlo simulation in the preceding section and Π for various combinations of N, s, τ and γ, P_{ij} values have been calculated. Examples of P_{ij} for the present experiment are tabulated in table 6.

The observed intensity $\Delta I_j(\theta_k)$ of size N_j in ΔN is the sum of the intensity from various sizes N_i and is given by

$$\Delta I_j(\theta_k) = \sum_i P_{ij} \Delta I(N_i, \theta_k) \Pi(N_i, \theta_k).$$

Furthermore, some fraction of showers of zenith angle θ_k in $\Delta\theta$ is determined to be showers of zenith angle θ_l in $\Delta\theta$, due to the uncertainty of the zenith angle determination. Since this uncertainty can be expressed by a gaussian function of standard deviation $\sigma_{ZA}(\theta_k)$, the intensity at zenith angle θ_l in $\Delta\theta$ from the showers of θ_k in $\Delta\theta$ in shower size N_j in ΔN is

$$I_{jl}(\theta_k) = \frac{\Delta I_j(\theta_k)}{(2\pi)^{1/2}\sigma_{ZA}} \int_{\theta_l}^{\theta_l + \Delta\theta} \exp\left\{-\frac{1}{2}\left(\frac{\theta_k - \theta}{\sigma_{ZA}(\theta_k)}\right)^2\right\} d\theta.$$

By adding the contribution of all k, we obtain the intensity of showers of observed size N_j in ΔN and observed zenith angle θ_l in $\Delta\theta$ as

$$I_{jl} = \sum_k I_{jl}(\theta_k).$$

References

Adair R K and Price N J 1966 *Phys. Rev.* **142** 844–51

Amineva T P *et al* 1971 *Proc. 12th Int. Conf. on Cosmic Rays, Hobart* vol 6 (Hobart: University of Tasmania) pp 2387–96

Asbury J G, Cooper W A, Voyvodic L, Walker R J and Wangler T P 1970 *Nuovo Cim.* B **66** 169–82

Baradzei L T, Kanevskaya E A, Smorodin Yu A and Soloviyev M V 1971 *Proc. 12th Int. Conf. on Cosmic Rays, Hobart* vol 6 (Hobart: University of Tasmania) pp 2397–407

Bergeson H E, Keuffel J W, Larson M O, Martin E R and Mason G W 1967 *Phys. Rev. Lett.* **19** 1487–91

Bergeson H E *et al* 1971 *Proc. 12th Int. Conf. on Cosmic Rays, Hobart* vol 4 (Hobart: University of Tasmania) pp 1418–22

Bjorken J D, Pakvasa S, Simmons W and Tuan S F 1969 *Phys. Rev.* **184** 1345–55

Böhm E *et al* 1970 *Acta Phys. Hung.* **29** *Suppl.* 4 121–4

Böhm E, Nagano M, van Staa R and Trümper J 1971 *Proc. 12th Int. Conf. on Cosmic Rays, Hobart* vol 4 (Hobart: University of Tasmania) pp 1438–44

Böhm E, Roose U J, Staubert R and Trümper J 1966 *Nucl. Instrum. Meth.* **40** 67–72, 73–6

Castagnoli C, Etim E and Picchi P 1969 *Lett. Nuovo Cim.* **1** 197–200

Carlson G W, Keuffel J W and Morrison J L 1971 *Proc. 12th Int. Conf. on Cosmic Rays, Hobart* vol 4 (Hobart: University of Tasmania) pp 1412–7

Catz Ph, Gawin J, Hochart J P, Maze R and Wdowczyk J 1971 *Proc. 12th Int. Conf. on Cosmic Rays, Hobart* vol 3 (Hobart: University of Tasmania) pp 1030–4

Chin S *et al* 1971 *Proc. 12th Int. Conf. on Cosmic Rays, Hobart* vol 4 (Hobart: University of Tasmania) pp 1468–74

Dedenko L G and Zhelenznykh I M 1971 *Proc. 12th Int. Conf. on Cosmic Rays, Hobart* vol 6 (Hobart: University of Tasmania) pp 2201–10

Erlykin A D 1965 *Proc. 9th Int. Conf. on Cosmic Rays, London* vol 2 (London: The Institute of Physics and The Physical Society) pp 999–1002

Faissner H *et al* 1970 *Phys. Rev. Lett.* **24** 1357–60

Flatté S M, Decoster R J, Stevenson M L, Toner W T and Zipf T F 1971 *Phys. Lett.* **35B** 345–50

Gawin J, Maze R and Wdowczyk J 1970 *Proc. 6th Interam. Sem. on Cosmic Rays, La Paz* vol 3 (La Paz: University of San Andres) pp 723–39

Gell-Mann M 1964 *Phys. Lett.* **8** 214–5
Greisen K 1956 *Progress in Cosmic Ray Physics* vol 3 (Amsterdam: North Holland) pp 17–8
Hara T *et al* 1970 *Acta Phys. Hung.* **29** *Suppl.* 4 125–31
Hayakawa S 1969 *Cosmic Ray Physics* (New York: Wiley) p 467
Higashi S *et al* 1961 *Nuovo Cim.* **22** 304–7
Kendziorra E 1971 *Dipl. Thesis* University of Kiel
Khristiansen G B *et al* 1965 *Proc. 9th Int. Conf. on Cosmic Rays, London* vol 2 (London: The Institute of Physics and The Physical Society) pp 799–801
Khristiansen G B, Vedeneev O V and Nechin Yu A 1971 *Proc. 12th Int. Conf. on Cosmic Rays, Hobart* vol 6 (Hobart: University of Tasmania) pp 2122–31
Király P and Wolfendale A W 1970 *Phys. Lett.* **32B** 510–2
Király P, Thompson M G and Wolfendale A W 1971 *J. Phys.* A: *Gen. Phys.* **4** 367–76
Kobayakawa K 1966 *Nuovo Cim.* **47** 156–94
Koshiba M, Nozaki T, Totsuka Y and Yamada S 1967 *J. Phys. Soc. Japan* **22** 1321
Krishnaswamy M R *et al* 1968 *Phys. Lett.* **27B** 535–8
Lee T D 1965 *Nuovo Cim.* **35** 933–44
Maeda K 1970 *Acta Phys. Hung.* 29 *Suppl.* 4 139–49
Matano T *et al* 1965 *Phys. Rev. Lett.* **15** 594–6
Matano T *et al* 1968 *Can. J. Phys.* **46** 369–72
Menon M G K and Ramana Murthy P V 1967 *Progress in Elementary Particle and Cosmic Ray Physics* vol 9 (Amsterdam: North Holland) pp 163–243
Mikamo S, Mizutani K and Mori K 1970 *Tokyo INS Report* 160
Miura I and Hasegawa H 1962 *J. Phys. Soc. Japan* **17** *Suppl.* A3 84–6
Mizutani K, Shirai T, Akashi M and Watanabe Z 1971 *Proc. 12th Int. Conf. on Cosmic Rays, Hobart* vol 4 (Hobart: University of Tasmania) pp 1392–7
Nagano M, Hara T, Kawaguchi S, Mikamo S, Suga K, Tanahashi G and Matano T 1971 *J. Phys. Soc. Japan* **30** 33–55
Pakvasa S, Simmons W A and Tennakone K 1971 *Proc. 12th Int. Conf. Cosmic Rays, Hobart* vol 3 (Hobart: University of Tasmania) pp 1189–93
Roose U J 1965 *Nucl. Instrum. Meth.* **36** 333–4
Sitte K 1969 *Lett. Nuovo Cim.* **1** 252–5
Smorodin Yu A 1966 *Zh. eksp. teor. Fiz.* **51** 431–44
Stefanski R J, Adair R K and Kasha H 1968 *Phys. Rev. Lett.* **20** 950–2
van Staa R 1968 *Dipl. Thesis* University of Kiel
Wright A G 1973 *J. Phys.* A: *Math., Nucl. Gen.* **6** 79–92
Woidneck C P, Böhm E, Trümper J and de Villiers E J 1971 *Proc. 12th Int. Conf. on Cosmic Rays, Hobart* vol 3 (Hobart: University of Tasmania) pp 1038–42
Zweig G 1964 *CERN Report No* 8419/TH 412